Biochimica et Biophysica Acta 1838 (2014) 1911–1920

Contents lists available at ScienceDirect

Biochimica et Biophysica Acta

journal homepage: www.elsevier.com/locate/bbamem

Design of novel cell penetrating peptides for the delivery of trehalose into mammalian cells

Yuping Wei [a,b,1], Chunlong Li [a,b,1], Liang Zhang [a,b], Xia Xu [a,*]

[a] State Key Laboratory of Biochemical Engineering, Institute of Process Engineering, Chinese Academy of Sciences, Beijing, PR China, 100190
[b] University of Chinese Academy of Sciences, Beijing 100049, China

ARTICLE INFO

Article history:
Received 16 September 2013
Received in revised form 13 February 2014
Accepted 19 February 2014
Available online 26 February 2014

Keywords:
Cell penetrating peptide
Trehalose
Stabilization
Lyophilization
Mammalian cell

ABSTRACT

Stabilization of cells in a desiccated state can significantly simplify the storage and transportation and save expenses for clinical applications. Introduction of the impermeable disaccharide, trehalose, into cells is an important step to improve the desiccation tolerance of cells. In this study, a novel cell penetrating peptide, KRKRWHW, was developed based on molecular simulations. The peptide exhibited little cytotoxicity and high penetrating efficiency into mammalian cells. The cell viability of mouse embryonic fibroblasts (MEFs) after the incubation with various concentrations of KRKRWHW from 0.01 mM to 5 mM at 37 °C for 4 h was maintained at around 100%. The peptide was able to penetrate into MEFs within 1 h at 37 °C with an efficiency of around 90% at 0.1 mM. Trehalose, as a cargo coupled with the peptide of KRKRWHW through hydrogen bond and π–π bond, was successfully loaded into the MEFs. This novel peptide provides a novel approach for the delivery of trehalose into mammalian cells.

1. Introduction

Stabilization of cell-based products has become a critical barrier against their successful commercialization in tissue engineering and cell therapy etc. [1]. Lyophilization and cryopreservation have been widely used to stabilize cells and tissues to ensure the off-the-shelf availability during long-term storage [2]. Due to constraints in the storage and transportation at cryogenic temperature in cryopreservation [3], storage of cells in the desiccated state would greatly simplify the storage and transportation and facilitate their applications in clinical therapies.

Trehalose as a non-reducing disaccharide having a high glass transition temperature and a dihydrate crystalline structure has been demonstrated to be able to increase the stability of dried liposomes [4], bacteria [5], yeast and retrovirus [6] and platelets [7]. The stabilization mechanism provided by trehalose is not fully elaborated. It has been suggested that trehalose may replace the water shell around macromolecules to prevent protein aggregation and denaturation [2], depress the phase transition temperature of membranes to remain membrane integrity during drying [8,9], and form stable glasses during freeze-drying [10].

Introduction of trehalose into cells is an important step to provide protection against cell damage during lyophilization [11]. In recent years numerous approaches have been developed to load trehalose into mammalian cells to improve desiccation tolerance, including passive trehalose influx by microinjection [12], genetically engineered pores [11–13], thermal shock and osmotic shock [14], transient membrane leakage at the phase transition temperature [15], and fluid-phase endocytosis [16]. The major drawback with these methods is that the processes of intracellular delivery are not trehalose specific, which may further result in the loss of intracellular components through the open pores. In addition, gene expression biosynthesis of trehalose using a recombinant adenovirus vector has been applied to introduce trehalose into human primary fibroblasts [17]. However, this may raise concerns on the risk during clinical applications. Hence, it is necessary to develop a novel method to specifically deliver trehalose into cells without causing damage to the cells.

Cell penetrating peptides (CPPs), rich in basic amino acids, are short peptides which can translocate through cell membranes and can be conjugated with a cargo, such as oligonucleotides [18], plasmids [19], proteins [20], and enter living cells [21]. The mechanism behind the translocation is still unclear; presumably endocytosis plays an important role in the translocation especially when cargo molecules are conjugated [22]. Since CPPs can deliver the specific cargo into the cells and no intracellular components escape from the cells, CPPs have been widely used to deliver a variety of cargos into cells without entrapment in lysosome [23,24]. However, due to the cytotoxicity of CPPs and the

Abbreviations: CPP, Cell penetrating peptide; DAPI, 4′,6-diamidino-2-phenylindole; DIEA, N,N-Diisopropylethylamine; DMEM, Dulbecco's Modified Eagle's medium; DMF, N,N-Dimethylformamide; EDT, 1,2-eth-anedithiol; FITC, fluorescein isothiocyanate; HOBt, 1-Hydroxybenzotriazole; MEF, mouse embryonic fibroblast; MTT, dimethyl thiazolyl diphenyl tetrazolium salt; PI, propidium iodide; RMSD, root mean square deviation; TBTU, O-(Benzotriazol-1-yl)-N,N,N′,N′-tetramethyluronium tetrafluoro-borate; TFA, trifluoroacetic acid; TIS, triisopropylsilane

* Corresponding author at: No. 1 Beiertiao, Zhongguancun, Haidian District, Beijing 100190, PR China. Tel.: +86 1082544939; fax: +86 82544939.
E-mail address: xuxia@home.ipe.ac.cn (X. Xu).

[1] These authors have contributed equally to this work.

http://dx.doi.org/10.1016/j.bbamem.2014.02.011
0005-2736/

difficulty in efficient release of the covalent conjugated target molecules, an alternative CPP offering low cytotoxicity and efficient intracellular delivery of target molecules needs to be developed.

In this study, a CPP was designed based on the molecular docking and dynamics simulations and synthesized in order to provide a more effective and specific technique for intracellular delivery of trehalose. The novel CPP is rich in basic amino acid and contains several amino acids having the ability of coupling with trehalose through non-covalent bonding. We evaluated the cytotoxicity of the novel CPP and further examined the efficiency of the CPP entering into living MEFs. The capacity of intracellular trehalose loading using the CPP was also determined. Our results reveal that the designed CPP exhibits little cytotoxicity and a high efficiency of intracellular trehalose delivery.

2. Materials and methods

2.1. Materials

Peptide synthesis reagent O-(Benzotriazol-1-yl)-N,N,N′,N′-tetramethyluronium tetrafluoro-borate (TBTU), N,N-Dimethylformamide (DMF), 1-Hydroxybenzotriazole (HOBt), N,N-Diisopropylethylamine (DIEA), isopropanol, trifluoroacetic acid (TFA), phenol, thioanisole, 1,2-eth-anedithiol (EDT), piperidine were purchased from DaTianFengTuo Chem (Beijing, China). Amino acids and Wang resins used in peptide synthesis were purchased from GL Biochem (Shanghai, China). Trehalose was purchased from Yuanye Bio-Technology (Beijing, China), fluorescein isothiocyanate (FITC) from Merck (USA) and dimethyl thiazolyl diphenyl tetrazolium salt (MTT) from Amresco (USA). Fetal bovine serum (FBS), trypsin, Dulbecco's Modified Eagle's medium (DMEM), phosphate buffered saline (PBS), L-glutamine and nonessential amino acid were purchased from Hyclone (USA). Paraformaldehyde and 4′,6-diamidino-2-phenylindole (DAPI) were purchased from Sigma (USA). Calcein-AM and propidium iodide (PI) were purchased from Fanbo Biochemicals (Beijing, China).

2.2. Design of CPPs

The structures of trehalose (TRE) and heparin sulfate (1HPN) were downloaded from the RCSB protein data bank (PDB). The structure of polypeptides utilized in the molecular simulations was sketched using the Discovery Studio Visualizer (DSV) 3.0. Topology and parameters of force field for the trehalose and heparin sulfate were generated using the PRODRG2 server (http://davapc1.bioch.dundee.ac.uk/cgi-bin/prodrg_beta) [25]. Molecular docking using the AutoDock 4.0 with Lamarckian Genetic Algorithm (LGA) was carried out to investigate the interactions between the designed peptides and trehalose and heparin sulfate. Except for a maximum number of 2,500,000 energy evaluations and 100 runs in $60 \times 60 \times 60$ grid box with spacing at 0.375 Å, all the other parameters were set as the default.

Molecular dynamics (MD) simulations were carried out using the GROMACS 4.5.4 and the standard GROMOS96 force field. Long-range electrostatics interactions were treated by the Particle Mesh Ewald (PME) [26]. The peptide was first immersed in a box containing the Simple Point Charge (Extended) water model, and then the trehalose and heparin were subsequently added into the system. Each system for the simulations was neutralized by adding Na^+ or Cl^-. Before each system was equilibrated for 20 ps, an energy minimization was employed. For each system, the simulation was performed at 300 K, physiological pH and 1 atm for a total of 10 ns to assess the stability of the tested systems. The system stability was verified by analyzing the energy components and the root mean square deviation (RMSD) of the structures in the trajectory compared to the starting conformation. The simulation results were visualized using the Visual Molecular Dynamics (VMD) and DSV. All computing was performed on the Lenovo ThinkStation E30 (Lenovo, China).

2.3. Synthesis of CPPs

Peptides were synthesized manually on a Wang resin using the standard Fmoc solid-phase synthesis strategy [27]. Fmoc was removed by DMF containing 20% (v/v) piperidine for up to 30 min, followed by three washes in isopropanol and DMF at room temperature, respectively. Stepwise coupling of Fmoc-amino acids to the growing peptide chain on the resin was performed in the reaction mixture of TBTU 0.91 g, DMF 10 ml, HOBt 0.45 g and 0.52 ml DIEA at room temperature for 2 h. After each amino acid was added, the step of deprotection of Fmoc group was performed. After the last amino acid was added to the peptide chain, the cleavage of peptide from the resin was carried out in the mixture of TFA, triisopropylsilane (TIS), H_2O and EDT (94:1:2.5:2.5, v/v) at 0 °C ice-water while being stirred at 3000 rpm. All crude peptides were purified using a reverse-phase high performance liquid chromatography (RP-HPLC, LC-8A, SHIMADZU, Japan) on a C18 column to purity >95%. The identity of the purified peptides was determined using a MALDI-TOF mass spectrometer (Autoflex III LRF200-CID, Bruker, Germany). To visualize the penetration of CPPs, the C-terminal of the CPP was conjugated with FITC, a fluorescence tag, at the R group of Lys when synthesized.

2.4. Cell culture

MEF cells were cultured and maintained in complete culture medium, DMEM supplemented with 10% FBS, 1% nonessential amino acids and 1% L-glutamine. All cells were incubated in a 5% CO_2 humidified atmosphere at 37 °C.

2.5. Cytotoxicity and cell viability assays

Cytotoxicity was assessed using the MTT assay. The MEF cells were seeded at 8000 cells/well in 96-well plates and cultured for 24 h before treatment. The cells were incubated in the serum-free culture medium with various concentrations of peptides in the range from 0.01 mM to 5 mM for 4 h in a 5% CO_2 humidified atmosphere at 37 °C. To investigate the effect of trehalose loaded by the designed CPPs on the cell metabolic rate, the cells were incubated with the CPP and trehalose together for 2 h in a 5% CO_2 humidified atmosphere at 37 °C. The concentration of the CPP was 1 mM, and the ratio of the CPP to trehalose was set at 1:8. The cytotoxicity was determined immediately after the incubation and after subsequent 24 h of culture by the MTT assay. For the MTT assay, MTT was added to the tested wells at the final concentration of 1 mg/ml and incubated for 4 h at 37 °C and then 100 μl of DMSO was added to the wells after the medium was removed. The absorbance was determined using a microplate reader (Infinite F20, Tecan, Switzerland) at 490 nm. The cells cultured with the normal medium were used as the negative control.

Cell viability of adherent MEFs before and after the incubation with the CPP was evaluated using the Calcein-AM and PI staining method. Briefly, the cells were seeded at the density of 4×10^4 cells/well onto 15 mm of coverslips in 24-well plates and incubated with the medium containing the CPP only or the CPP together with trehalose for 24 h. The cells immediately after the incubation with the CPP or the CPP together with trehalose and after subsequent 24 h culture with normal medium were stained with 1 μM Calcein-AM and 2 μM PI for 10–15 min in the dark, and then washed with PBS for three times. The green and red fluorescence in the stained cells were visualized using a fluorescence microscope (Nikon, Japan) excited at 488 nm and 535 nm, respectively, connected to an imaging capture system (Tucsen, China). The cell morphology was visualized using a microscope.

2.6. The cellular uptake assay of CPPs

The MEF cells were seeded onto the coverslips with a diameter of 15 mm in 24-well plates at the density of 4×10^4 cells/well and cultured for 24 h. After the incubation with the serum-free culture medium

Table 1
Docking results for heparin and different peptides containing three to six Arg (kcal/mol).

System	Intermolecular energy		Torsional free energy	Internal energy	Binding free energy
	VDW-HB -DESOLVE[a]	Electrostatic energy			
RRR	−8.53	−12.27	4.49	−1.47	−13.54
RRRR	−8.29	−15.15	6.59	−1.6	−17.2
RRRRR	−8.77	−16.89	8.23	−1.33	−16.94
RRRRRR	−9.72	−19.29	9.88	0.47	−16.7

[a] indicates van der Waals, H-bond and desolvation energy.

containing FITC-labeled peptides or FITC-only at the concentrations of 0.01, 0.1, 0.2 and 0.5 mM for 1 h in a 5% CO_2 humidified atmosphere at 37 °C, the cells were washed with PBS, fixed with 4% paraformaldehyde, and then stained with DAPI. After three times washing with PBS, the green fluorescence in the stained cells was visualized using a fluorescence microscope excited at 488 nm connected to an imaging capture system. The cells show the green fluorescence once the peptides conjugated with FITC are translocated into the cells. To test the penetration of KW over time, we observed the green fluorescence of cells after the incubation with KW-FITC at the concentration of 0.2 mM for 5 min and 20 min using a fluorescence microscope (Nikon, Japan). To determine the intracellular distribution of this CPP, the cells were incubated with KW-FITC (0.2 mM) for 30 min and then the green fluorescence was observed using a confocal microscope (Leica, Germany). To evaluate the uptake efficiency, the cells were washed with PBS and digested using trypsin after the incubation with the FITC-labeled peptides or FITC-only. The cells were collected, centrifuged and resuspended in PBS. The ratio of the cells with green fluorescence to the cells without green fluorescence was taken as the uptake efficiency which was determined using a flow cytometer (Cyflow Cube6, Partec, Germany). The cells incubated with the normal culture medium were used as the negative control.

2.7. Intracellular delivery of trehalose

To eliminate interference from the presence of glucose in the culture medium when measuring the intracellular concentration of trehalose, the glucose-free culture medium was used here. The designed CPP (1 mM) was added into the glucose-free culture medium, and then the trehalose was introduced at the molar ratio of 1:8. The cells were incubated in the glucose-free culture medium containing both the CPP and trehalose or trehalose-only for 2 h in a 5% CO_2 humidified atmosphere at 37 °C. After the incubation the cells were washed twice with PBS and left at 4 °C for 30 min to detach the cells from the adherent surface. The cells suspended in PBS were counted using a flow cytometer. The cells cultured in the glucose-free medium with trehalose-only were used as the positive control and the cells cultured in the glucose-free culture medium were used as the negative control. The trehalose concentration was determined by the anthrone reaction [28]. Briefly, the cells were lysed by a freeze-thawing method. The cell debris was removed through a 0.22 μm filter. For the trehalose quantification, the trehalose solution was mixed with anthrone reagent, boiled for 10 min, and then allowed to cool. The absorbance at 620 nm was read using a microplate reader and compared with a standard curve. The trehalose concentration for a single cell was calculated by the mole of trehalose to the cell volume. Usually the radius of cells is 7–10 μm, therefore here we regarded the cells as sphere and calculated the cell volume using the radius of 7 μm. The cell number was counted using a flow cytometer.

2.8. Statistical analysis

Unless indicated otherwise, at least three independent experiments were conducted for each tested condition. Data are presented as means ± standard deviation (sdev) for the experiments. One-way analysis of variance (ANOVA) was performed to determine statistical significance ($p < 0.05$).

3. Results and discussion

3.1. CPP design

3.1.1. Residues interacting with heparin

Heparin, a highly sulfated glycosaminoglycan with negative charge, is a member of the glycosaminoglycan family of carbohydrates and consists of a variably sulfated repeating disaccharide unit with a molecular

Table 2
Docking results for heparin and peptides composed of Arg and Lys with various combinations (kcal/mol).

System	Intermolecular energy		Torsional free energy	Internal energy	Binding free energy
	VDW-HB -DESOLVE	Electrostatic energy			
RKKK	−10.2	−18.2	7.41	0.01	−19.51
KRKR	−8.04	−17.98	7.13	−0.45	−17.85
RRKK	−5.73	−19.89	7.13	−0.5	−17.51
RRRR	−8.29	−15.15	6.59	−1.6	−17.2
KKKK	−9.19	−16.3	8.35	−0.95	−17.14
KRRK	−8.43	−16.38	7.13	−0.62	−17.11
RRKR	−8.29	−15.17	6.86	−1.69	−16.8
KKRK	−8.08	−16.98	7.41	−0.29	−16.45
KRKK	−7.44	−15.59	7.41	−1.98	−16.1
RKRK	−9.15	−14.87	7.13	−0.71	−16.1
RRRK	−6.79	−14.69	6.86	−2.92	−16.06
KRRR	−7.25	−15.67	6.86	−1.38	−15.94
KKKR	−6.97	−17.15	7.41	−0.76	−15.93
KKRR	−6.25	−16.01	7.13	−2.07	−15.69
RKKR	−8.37	−14.65	7.13	−1.32	−15.69
RKRR	−7.5	−15.21	6.86	−1.03	−15.37

Table 3
Docking results for trehalose and peptides composed of Trp and His with various combinations (kcal/mol).

System	Intermolecular energy		Torsional free energy	Internal energy	Binding free energy
	VDW-HB -DESOLVE	Electrostatic energy			
WWH	−7.4	−0.76	3.58	−2.57	−4.64
WHH	−5.15	−0.6	3.29	−3.38	−4.55
HHW	−4.18	−0.63	3.29	−4.13	−4.35
WHW	−7.12	−0.46	3.58	−1.63	−4
HWW	−6.7	−0.62	3.58	−2.54	−3.8
WWW	−5.02	−0.42	3.58	−2.23	−3.64
HWH	−4.52	−0.4	3.29	−3.29	−3.42
HHH	−6.12	−0.76	3.58	−1.84	−3.31

weight ranging from 3 kDa to 30 kDa [29]. The main disaccharide units in heparin are composed of a 2-O-sulfated iduronic acid and 6-O-sulfated and N-sulfated glucosamine. Since heparin sulfates are present on the plasma membrane, in this study heparin was used as a receptor of peptide–trehalose complex for designing CPPs based on the interactions between heparin and CPPs.

Cationic charges of peptide play a critical role in cell penetration [30,31], especially the guanidinium group of the arginine (Arg, R) side chain [32]. Therefore, the sequence of peptides was constructed and the effect of the number of Arg residues in the peptides on the interactions between the peptides and heparin was investigated using the AutoDock. For the running of AutoDock, an empirical scoring system was employed base on the binding free energy including the intermolecular energy, internal energy, torsional free energy and unbound system energy. The binding free energies and the specific interaction between CPPs and heparin could be used as a guideline for the design of new CPPs [33]. As shown in Table 1, as expected, the electrostatic energy was increased with the number of Arg in the sequence of the designed peptides. However, the peptide RRRR had the lowest internal energy and binding free energy than the other polyarginines in molecular docking, indicating that the peptide RRRR having four residues probably had the most stable conformation and the strongest interaction between RRRR and heparin. Hence, the peptide RRRR was initially selected as the potential ligand for heparin.

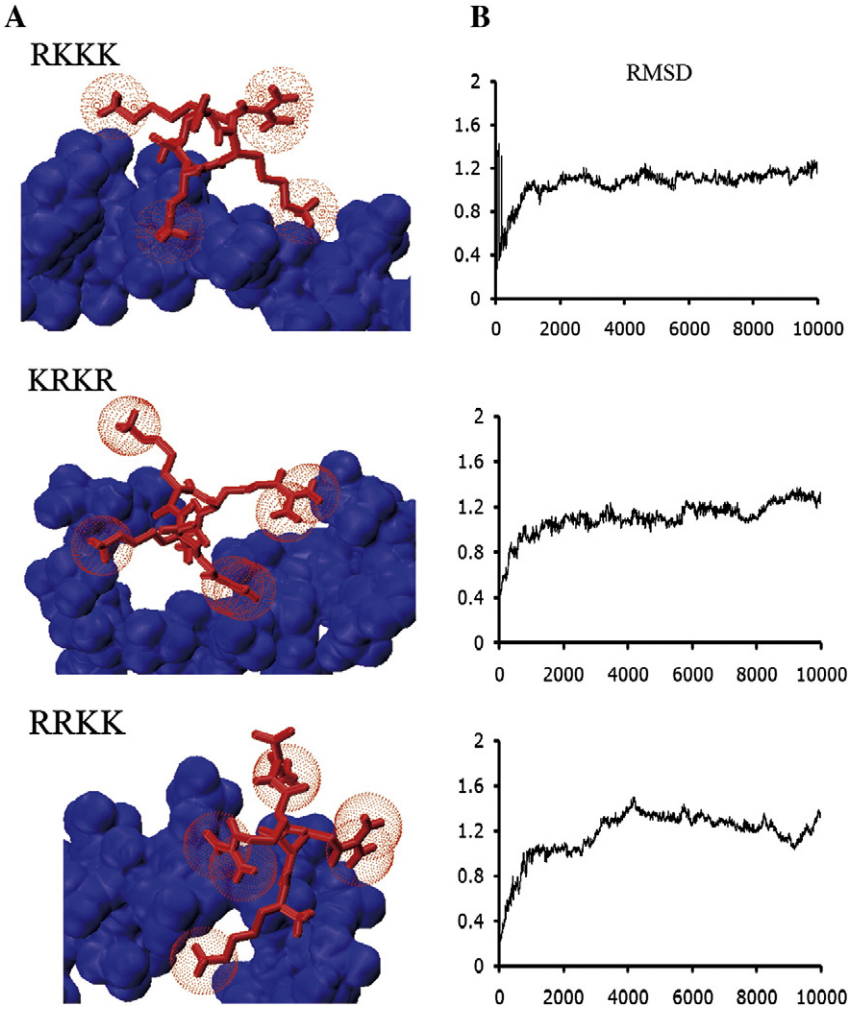

Fig. 1. Molecular dynamics simulations for the system of peptide–heparin. (A) Snapshots from a simulation trajectory of peptide–heparin at 10 ns. (B) RMSD during the MD simulations. Heparin is indicated in blue, and the peptides of RKKK, KRKR and RRKK in red.

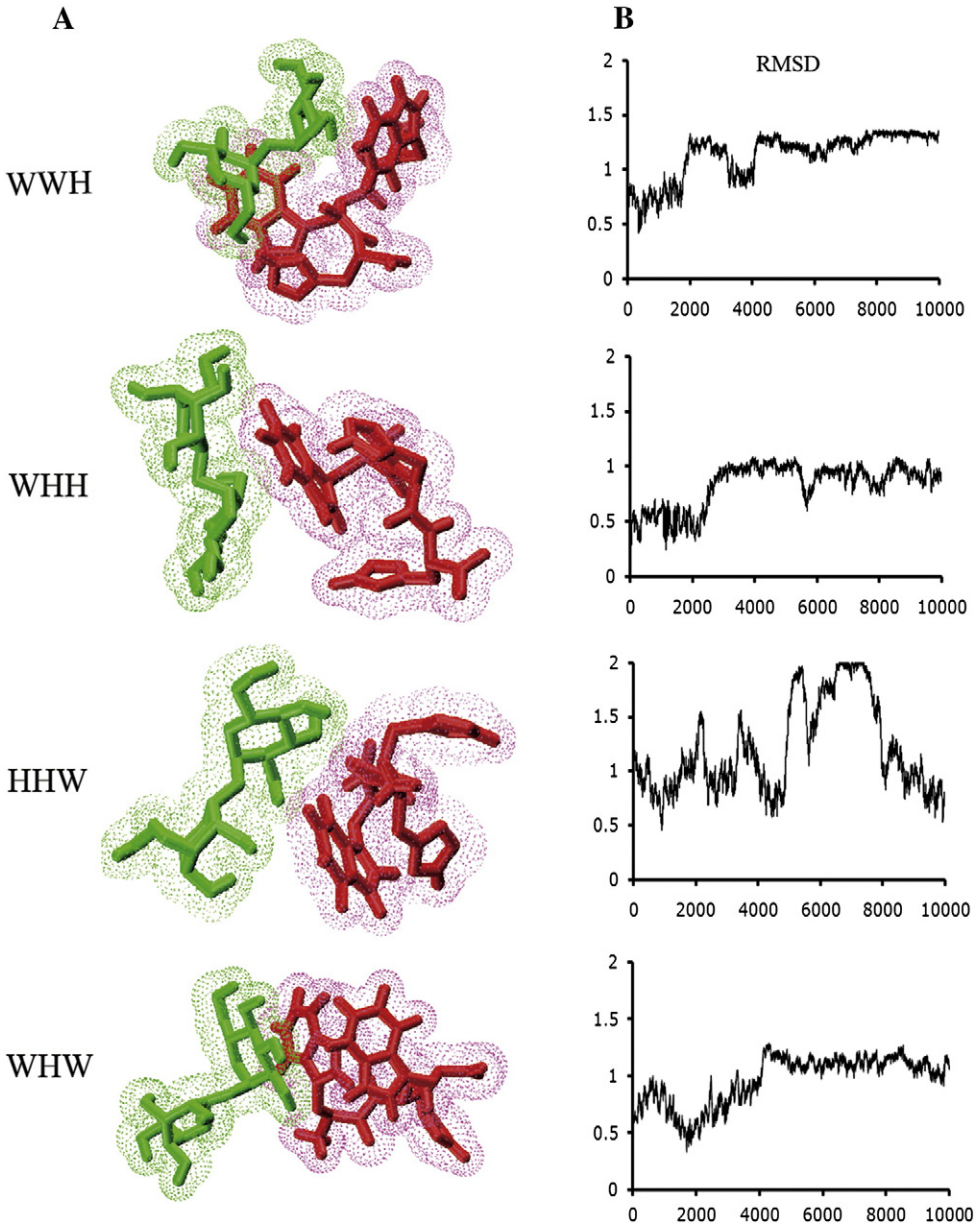

Fig. 2. Molecular dynamics simulations for the system of peptide–trehalose. (A) Snapshots from a simulation trajectory of peptide–trehalose at 10 ns. (B) RMSD during the MD simulations. Trehalose is indicated in green, and the peptides of WWH, WHH, HHW and WHW in red.

It has been reported that lysine (Lys, K) has a potential for mediating cell uptake [34] and that the CPPs rich in Arg are difficulty in synthesis [35]. Therefore, a combination of Arg and Lys groups was simulated to seek the potential candidates for cell penetration. The docking results for the system of heparin–peptide were listed in Table 2. Considering the binding free energy and the electrostatic energy, the peptides of RKKK, KRKR, RRKK were chosen as the potential candidates for achieving the function of cell penetration.

Table 4
Total free energy (kJ/mol) in the system of trehalose–peptide–heparin according to the molecular simulations.

Sequence	Total free energy among trehalose, peptide and heparin	Total free energy between peptide and trehalose
KRKRWHW	−83.0677	−48.89
KRKRWHH	−287.55	177.866
RKKKWHW	−133.023	−131.46

3.1.2. Residues interacting with trehalose

Trehalose was supposed to be delivered into mammalian cells by the designed CPP via a non-covalent strategy. Since tryptophane (Trp, W) and histidine (His, H) with the lowest binding free energy have aromatic R groups which can easily form hydrogen bond (H-bond) and hydrophobic interactions with trehalose [36], Trp and His were selected to be the potential amino acids composing the designed CPP for coupling trehalose via the non-covalent strategy. The interactions between peptides and trehalose were evaluated using the AutoDock, as shown in Table 3. Based on the binding free energy and the energy in combination of van der Waals, H-bond and desolvation energy, the peptides WWH, WHH, WHW and HHW were selected to couple trehalose through the non-covalent bonds.

3.1.3. Molecular dynamics simulations

A number of force fields have been developed in molecular dynamics simulation, such as CHARMM, AMBER, GROMOS, OLPLS and COMPASS. Although each force field has its particular strength and weakness on

the particular problem considered [37], all the leading forces provide reasonable results for a wide range of properties of isolated molecules, pure liquids and aqueous solutions [38]. The force field of GROMOS96 has been employed to simulate the interactions between peptide and trehalose [39,40], and between peptide and heparin [41,42]. To determine the conformation and stability of the systems, the molecular dynamics simulations for the system of peptide–trehalose and trehalose–peptide–heparin were performed using the Gromacs in a water environment at 300 K at 1 atm.

As shown in Fig. 1, the peptides RKKK and KRKR formed steady interactions with heparin, respectively, after 10 ns of simulation except for the peptide RRKK based on the fluctuation of RMSD. The results revealed that RKKK and KRKR could generate steady conformations with heparin whereas RRKK could not. We further simulated the interactions between the peptides of WWH, WHH and WHW and trehalose (Fig. 2). All the peptides of WWH, WHH and WHW formed steady interactions with trehalose after 10 ns of simulation except for the peptide HHW based on the fluctuation of RMSD and the positive value of the total free energy in the system of HHW–trehalose (data not shown), suggesting that the process is not spontaneous at constant pressure and temperature. Therefore the peptides of RRKK and HHW were eliminated from the candidate list for the further experiments.

After the above screening, six peptides were designed based on the combinations of the sequences of RKKK and KRKR with the sequences of WWH, WHH and WHW, respectively, for the further screening. We first evaluated the total free energy for the system of trehalose–peptide–heparin. However, only three peptides, KRKRWHW, KRKRWHH and RKKKWHW, had relatively low total free energy in the system of trehalose–peptide–heparin (Table 4). As shown in Fig. 3, there was little change in the RMSD after 10 ns for all the tested systems (Fig. 3A), revealing that the tested systems were in the steady status after 10 ns. These results suggest that they might have great potential for the interactions with trehalose and heparin. Therefore, these three peptides were chosen for the next step of design. However, it was interesting to note that the total free energy between KRKRWHH and trehalose was very positively high in the system of trehalose–peptide–heparin (Table 4), indicating that the interaction between KRKRWHH and trehalose in the system of trehalose–peptide–heparin is not favorable.

As shown in Fig. 3B, the trehalose was initially coupled with WHW at the preferred interaction sites in the system of trehalose–RKKKWHW, then migrated to the middle position of RKKKWHW once the heparin was added to the system (Fig. 3C). The simulation results revealed that the trehalose experienced the process of re-distribution along the

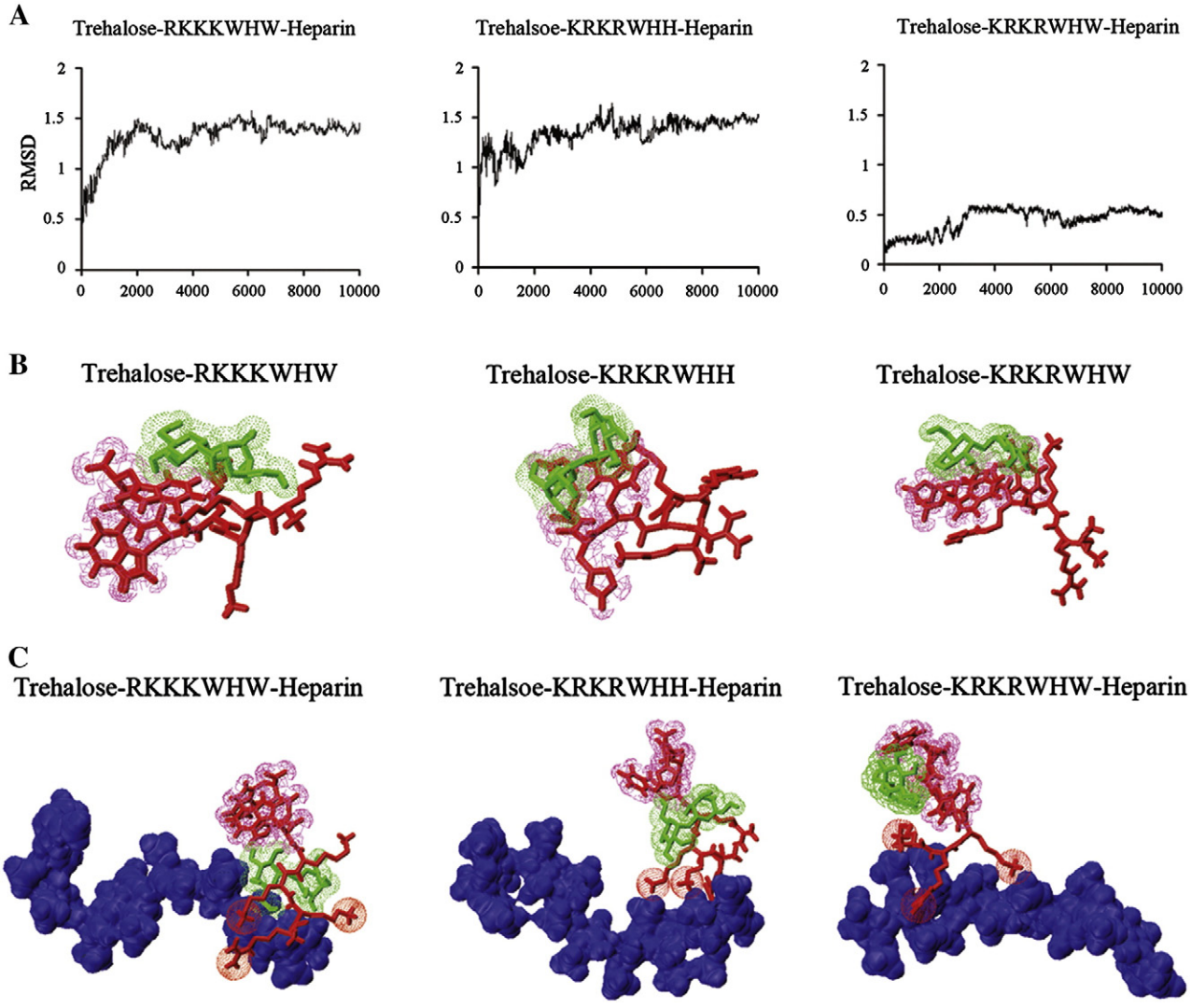

Fig. 3. The molecular simulations for trehalose–peptide–heparin. (A) The RMSD of the system containing trehalose, peptide and heparin. (B) The binding conformation of the system including trehalose and peptide. (C) The binding conformation of the system containing trehalose, peptide and heparin. Trehalose is indicated in green, peptides in red and heparin in blue.

peptide once the heparin was introduced into the system. In contrast, the trehalose still interacted with KRKRWHW at WHW as designed after the heparin was introduced into the system through the H-bond and π–π bond but not through the covalent bonding. Hence in this study, the sequence of KRKRWHW (hereafter referred to as KW) was finally selected as the potential CPP for the intracellular delivery of trehalose.

3.2. In vitro cytotoxicity of KW

The cytotoxicity of CPPs depends on the charge, hydrophobicity, length and structure [43], concentration, cargo molecule and coupling strategy [44]. To determine the cytotoxicity profile of KW, here the mammalian cells, mouse embryonic fibroblasts (MEFs), were evaluated at physiological pH by the MTT assay. The cytotoxicity was evaluated after 4 h of exposure to the various concentrations of 0.1, 0.5, 1, 2 and 5 mM KW at 37 °C in 5% CO_2. As shown in Fig. 4A, after 4 h of exposure to the culture medium containing KW, the presence of KW did not cause a significant decrease in the cell viability, even at 5 mM of KW, and nearly all the cells were viable for all the tested conditions. We further detected the cytotoxicity after 24 h of culture in the normal culture medium following 4 h of exposure to the medium containing KW. In comparison with the control, there was no significant change in the cell viability (Fig. 4B), and nearly all the cells were viable for the tested conditions (Fig. 4C), indicating that the CPP designed here had no significant cytotoxicity at physiological pH even at the concentration of 5 mM. The negligible cytotoxicity induced by KW may benefit from the short length of KW and its low cationic charge [30]. The low hydrophobicity in the domain of KW may be another contribution for the little cytotoxicity caused by KW.

3.3. Cellular uptake of KW

The structure and cationic content of CPP appear to be responsible for the cell membrane translocation property [45]. Here KW labeled with FITC (KW-FITC) was used to evaluate the efficiency of the CPP penetration. It has been demonstrated that the N-terminal of a CPP coupled with fluorescein can lead to the increased membrane destabilization and elevated cytotoxicity caused by the increase in the hydrophobic nature of the peptide tail [44]. Therefore, KW was coupled with fluorescein at the C-terminal. The extent of penetration is related to the incubation temperature and the extracellular concentration [46–48]. The cells at the seeding density of 4×10^4 cells/well were cultured in the presence of KW-FITC or FITC-only at the concentrations of 0.01 mM, 0.1 mM, 0.2 mM and 0.5 mM at 37 °C in 5% CO_2 for 1 h, respectively. The cellular uptake of KW was monitored using the fluorescence microscope and the efficiency was determined using the flow cytometer. As shown in Fig. 5A, the green fluorescence was observed for all the tested concentrations and the intensity was increased with the concentration of KW-FITC. In addition, the green fluorescence could be obviously observed even at 5 min and became stronger over time (Fig. 5B). Since the fluorescence was weak, and was faint for the confocal observation

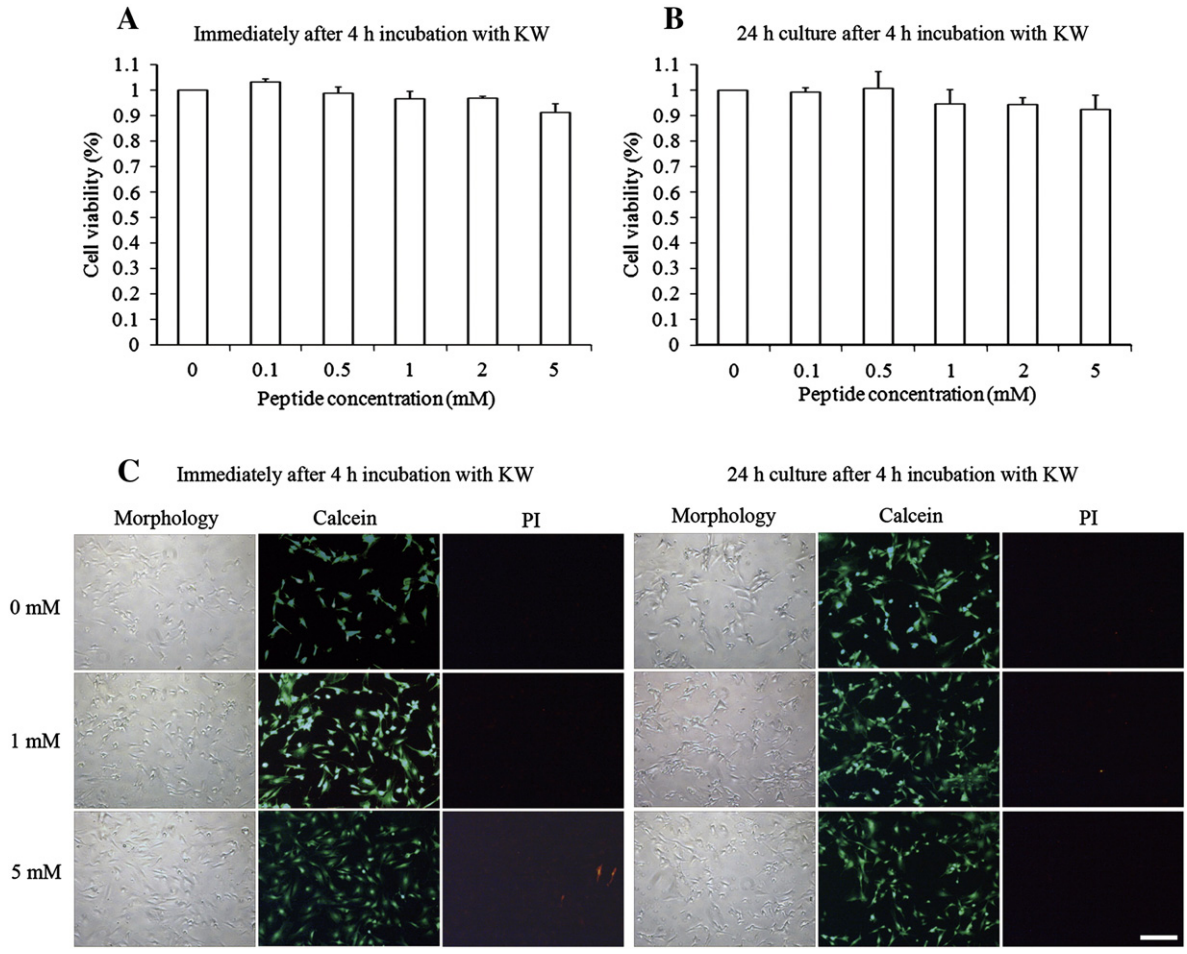

Fig. 4. The cytotoxic effects of KW on cell viability after incubation with various concentrations of KW in a 5% CO_2 humidified atmosphere at 37 °C. (A) The cell viability immediately after 4 h incubation with different concentrations of KW. (B) The cell viability after 24 h culture in the normal culture medium following 4 h exposure of various concentrations of KW. (C) The cell morphology and cell viability immediately and 24 h after 4 h incubation with various concentrations of KW. The cells were stained by Calcein-AM (1 μM) and PI (2 μM) and observed using a fluorescence microscope. Green: live cells, Red: dead cells. KW is short for the peptide of KRKRWHW. Bar = 200 μm.

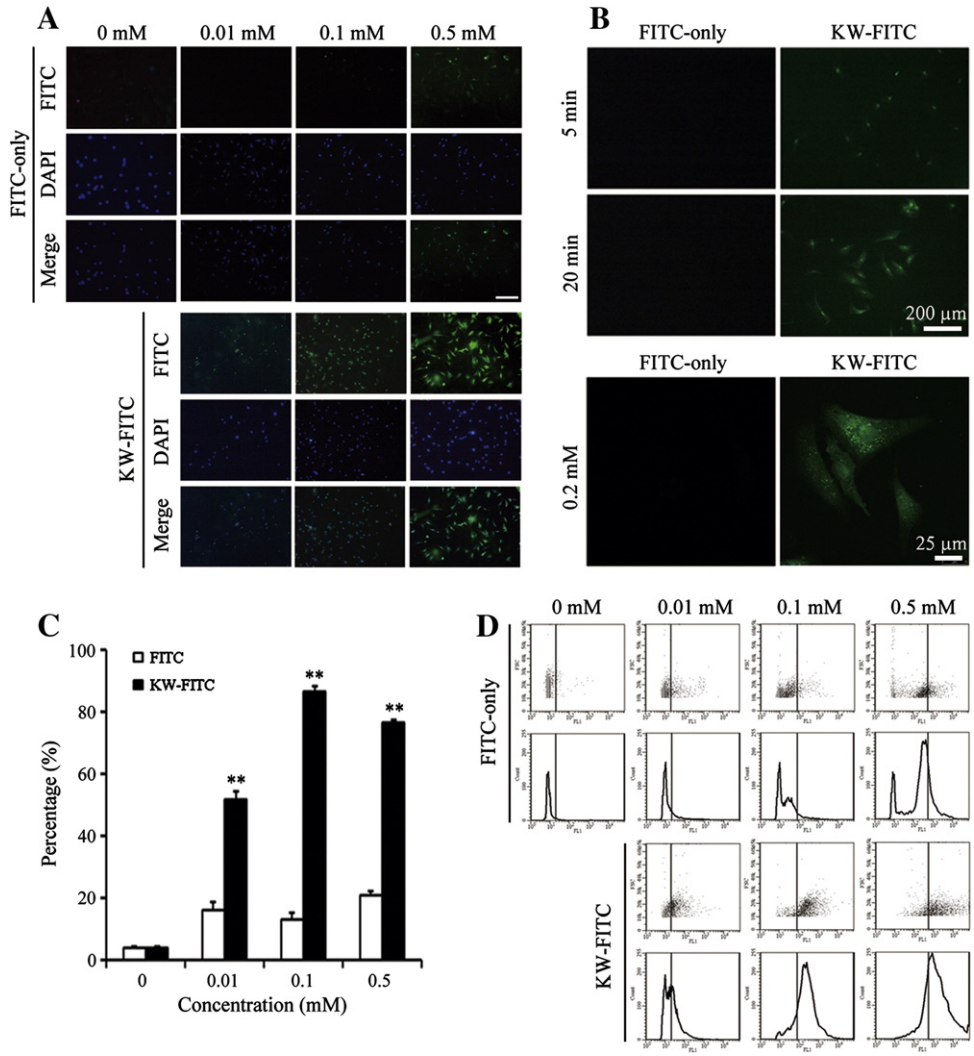

Fig. 5. The intracellular uptake of KW labeled with FITC. (A) Visualization of the translocation of various concentrations of KW-FITC. Bar = 200 μm. (B) The intracellular accumulation of KW-FITC over time and its distribution. Cells were incubated with KW-FITC at the concentration of 0.2 mM for 5 min and 20 min, respectively. The green fluorescence was observed using a fluorescence microscope. For the intracellular localization of KW-FITC, the cells were incubated with KW-FITC for 30 min and then the green fluorescence was observed using a confocal microscope. The cells incubated with FITC-only were used as the control. (C) The percentage of the cells containing KW-FITC tested by FACS analysis. (D) The representative results of FACS analysis. FITC-only was used as the controls. KW is short for the peptide of KRKRWHW. The asterisks (**, $p < 0.01$) indicate the significant difference.

at 0.001 to 0.01 mM, the result at 0.2 mM was presented. In contrast, the cells incubated with FITC-only did not show any visible green fluorescence. These results indicate that the peptide KRKRWHW can efficiently penetrate into cells. To determine the intracellular distribution of this CPP, the cells were incubated with KW-FITC for 30 min and then the green fluorescence was observed using the confocal microscope. The result showed that the green fluorescence was observed throughout the cells (Fig. 5B), implying that the peptides were located in the plasma and nuclear.

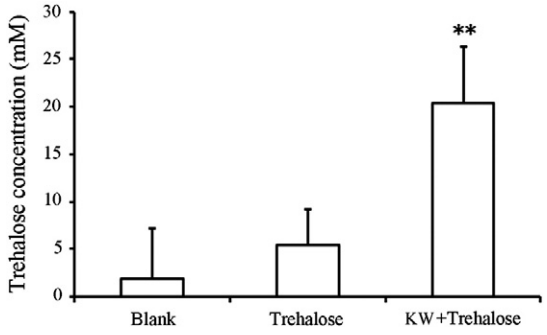

Fig. 6. The intracellular concentration of trehalose delivered by KW. The cells normally cultured (Blank) were used as the negative control. KW is short for the peptide of KRKRWHW. The asterisks (**, $p < 0.01$) indicate the significant difference.

At the concentration of 0.1 mM, nearly 90% of the cells were FITC positive (Fig. 5C), even at the concentration of 0.01 mM, around 60% of MEF cells appeared in green, indicating that the KW efficiently translocated into the cells without causing damages to the cell membranes (Fig. 4C). Usually the length required for an efficient arginine-rich CPP is greater than 8 amino acids. It is quite surprised that the CPP designed here, shorter than most CPPs, efficiently penetrated into mammalian cells, even within 5 min at the concentration of 0.2 mM as shown in Fig. 5B. With the help of the CPP, the FITC conjugated with the CPP was successfully translocated into the cells. In contrast, the FITC only did not penetrate into the cells. This indicates that the CPP described here has the capacity of penetration. The mechanism for the efficient penetration of KW needs to be elucidated further.

To avoid the false positive results caused by the cell membrane surface bound FITC, cells are usually treated with trypsin [22]. After digestion, the fluorescence activated cell sorting (FACS) results revealed that although there was a slight fluorescence signal generated by the FITC bound to the cell membranes, the fluorescence signal that was observed in the presence of KW-FITC was much stronger, indicating that the

peptides of KW were translocated and accumulated inside the cells (Fig. 5A and D). However, the surface bound FITC could not be completely removed by the trypsin digestion, hence a threshold for the fluorescence test was adjusted for each condition in comparison with the cells cultured with FITC-only medium (Fig. 5D). It should be noticed that this could have resulted in an underestimation of the uptake efficiency due to an overestimation of the number of the surface bound FITC.

3.4. Intracellular delivery of trehalose

The CPP is able to carry a diversity of molecules ranging from small molecules of some hundreds of Daltons to massive structures with a diameter up to 200 nm [49,50]. It is important to use appropriate CPPs for desired cargos since no single CPP is effective in delivery for all bioactive molecules [20,49]. The KW was designed to deliver trehalose into mammalian cells. During the simulations, the ratio of trehalose to KW was set at 1:1. When eight trehalose molecules were introduced into the simulation system, we found these trehalose grouped together though the H-bond and bound to the heparin (data not shown). Therefore, to evaluate the capacity of the trehalose loading, the trehalose (8 mM) with KW (1 mM) was loaded to the adherent MEF cells at physiological pH at 37 °C in 5% CO_2 for 2 h. Fig. 6 shows the intracellular trehalose concentration after 2 h incubation for all the tested conditions. In comparison with the cells incubated with trehalose only, there was a significant increase in the intracellular trehalose concentration when the KW and trehalose were both loaded. This implicated that the uptake of trehalose was mainly mediated by the CPP. A further study is needed to elucidate the mechanism behind the intracellular trehalose delivery with the help of KW.

To determine the intracellular concentration of trehalose, the cells must be lysed to release trehalose. Here, the freeze-thawing method was used to disrupt the cell membranes to release trehalose, which may lead to an underestimation of the intracellular trehalose concentration. In addition, the intracellular trehalose concentration may also be underestimated approximately by a factor of two due to not taking account of the osmotically inactive volume which is 56% of the isotonic cell volume [51].

Furthermore, dialysis was performed to determine the interactions between KW and trehalose, which confirmed that KW could bind trehalose (Supplementary content). The further experiments are needed to determine the loading limit of trehalose with the help of KW.

3.5. Cytotoxicity after KW translocation with trehalose

The cargo and the cargo-coupling position within the peptide also affect the cytotoxicity of the peptide [44]. We further tested the cytotoxicity after the trehalose was delivered into the cells using the designed CPP. The cytotoxicity was determined immediately and 24 h after trehalose loading. In comparison with the control, the trehalose loaded using the KW did not result in a loss in the cell viability, and the cells maintained their metabolic state and morphology (Fig. 7), suggesting that KW has the capacity of translocating trehalose into mammalian cells without causing cell death.

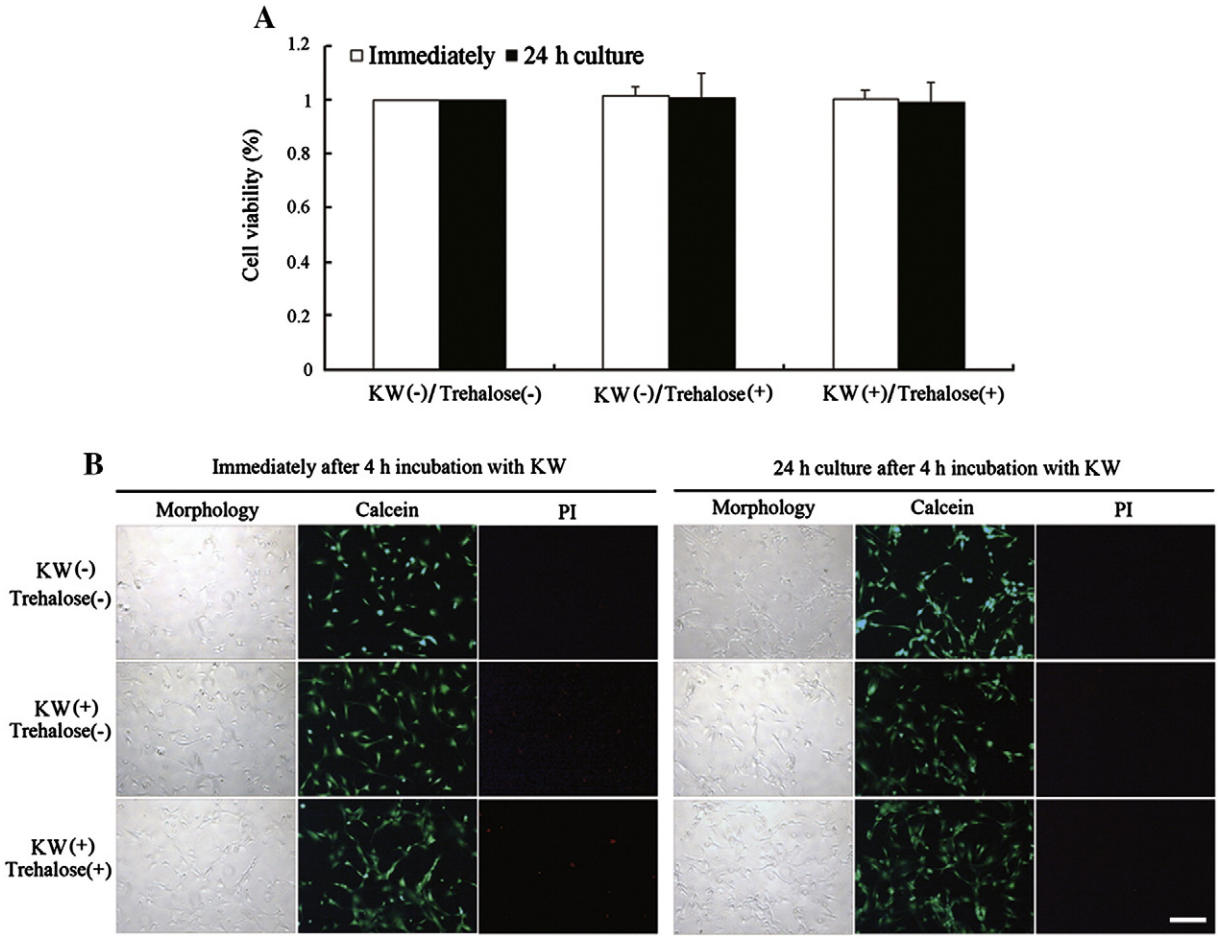

Fig. 7. The cytotoxicity of trehalose loaded by KW. (A) The cell viability after the incubation with KW and trehalose. (B) The cell morphology in (A) visualized after Calcein-AM (1 μM) and PI (2 μM) staining by a fluorescence microscope. The cell viability and morphology were determined immediately and 24 h after 4 h incubation with 1 mM KW. KW is short for the peptide of KRKRWHW. Green: living cells. Red: dead cells. Bar = 200 μm.

4. Conclusions

A novel cell penetrating peptide, KRKRWHW, was developed to deliver non-cell permeable trehalose into mammalian cells based on the molecular simulations. The CPP is able to efficiently deliver trehalose into mammalian cells with little cytotoxicity to mammalian cells even at high concentration. Therefore, this CPP may be very helpful for improving the desiccation tolerance of cells. The development of this CPP provides a novel approach for the delivery of trehalose into mammalian cells.

Acknowledgements

This research was supported by the Chinese Academy of Sciences, and the National Natural Science Foundation of China (21176238). The authors wish to thank the referees for helping to improve this manuscript during the review process.

Appendix A. Supplementary data

Supplementary data to this article can be found online at http://dx.doi.org/10.1016/j.bbamem.2014.02.011.

References

[1] J.O. Karlsson, M. Toner, Long-term storage of tissues by cryopreservation: critical issues, Biomaterials 17 (1996) 243–256.
[2] J.H. Crowe, L.M. Crowe, A.E. Oliver, N. Tsvetkova, W. Wolkers, F. Tablin, The trehalose myth revisited: introduction to a symposium on stabilization of cells in the dry state, Cryobiology 43 (2001) 89–105.
[3] P. Mazur, Freezing of living cells: mechanisms and implications, Am. J. Physiol. 247 (1984) C125–C142.
[4] W.Q. Sun, A.C. Leopold, L.M. Crowe, J.H. Crowe, Stability of dry liposomes in sugar glasses, Biophys. J. 70 (1996) 1769–1776.
[5] P.B. Conrad, D.P. Miller, P.R. Cielenski, J.J. de Pablo, Stabilization and preservation of *Lactobacillus acidophilus* in saccharide matrices, Cryobiology 41 (2000) 17–24.
[6] R.M. Bieganski, A. Fowler, J.R. Morgan, M. Toner, Stabilization of active recombinant retroviruses in an amorphous dry state with trehalose, Biotechnol. Prog. 14 (1998) 615–620.
[7] J.H. Crowe, F. Tablin, W.F. Wolkers, K. Gousset, N.M. Tsvetkova, J. Ricker, Stabilization of membranes in human platelets freeze-dried with trehalose, Chem. Phys. Lipids 122 (2003) 41–52.
[8] S.B. Leslie, S.A. Teter, L.M. Crowe, J.H. Crowe, Trehalose lowers membrane phase transitions in dry yeast cells, Biochim. Biophys. Acta 1192 (1994) 7–13.
[9] M.A. Singer, S. Lindquist, Multiple effects of trehalose on protein folding in vitro and in vivo, Mol. Cell 1 (1998) 639–648.
[10] J. Wolfe, G. Bryant, Freezing, drying, and/or vitrification of membrane–solute–water systems, Cryobiology 39 (1999) 103–129.
[11] T. Chen, J.P. Acker, A. Eroglu, S. Cheley, H. Bayley, A. Fowler, M. Toner, Beneficial effect of intracellular trehalose on the membrane integrity of dried mammalian cells, Cryobiology 43 (2001) 168–181.
[12] A. Eroglu, M.J. Russo, R. Bieganski, A. Fowler, S. Cheley, H. Bayley, M. Toner, Intracellular trehalose improves the survival of cryopreserved mammalian cells, Nat. Biotechnol. 18 (2000) 163–167.
[13] J.P. Acker, A. Fowler, B. Lauman, S. Cheley, M. Toner, Survival of desiccated mammalian cells: beneficial effects of isotonic media, Cell Preserv. Technol. 1 (2002) 129–140.
[14] I. Puhlev, N. Guo, D.R. Brown, F. Levine, Desiccation tolerance in human cells, Cryobiology 42 (2001) 207–217.
[15] W.F. Wolkers, N.J. Walker, F. Tablin, J.H. Crowe, Human platelets loaded with trehalose survive freeze-drying, Cryobiology 42 (2001) 79–87.
[16] A.E. Oliver, K. Jamil, J.H. Crowe, F. Tablin, Loading human mesenchymal stem cells with trehalose by fluid-phase endocytosis, Cell Preserv. Technol. 2 (2004) 35–49.
[17] N. Guo, I. Puhlev, D.R. Brown, J. Mansbridge, F. Levine, Trehalose expression confers desiccation tolerance on human cells, Nat. Biotechnol. 18 (2000) 168–171.
[18] M.J. Gait, Peptide-mediated cellular delivery of antisense oligonucleotides and their analogues, Cell. Mol. Life Sci. 60 (2003) 844–853.
[19] K. Rittner, A. Benavente, A. Bompard-Sorlet, F. Heitz, G. Divita, R. Brasseur, E. Jacobs, New basic membrane-destabilizing peptides for plasmid-based gene delivery in vitro and in vivo, Mol. Ther. 5 (2002) 104–114.
[20] J.S. Wadia, R.V. Stan, S.F. Dowdy, Transducible TAT-HA fusogenic peptide enhances escape of TAT-fusion proteins after lipid raft macropinocytosis, Nat. Med. 10 (2004) 310–315.
[21] K. Kilk, Cell-penetrating Peptides and Bioactive Cargos, Strategies and mechanisms, Stockholm University, Stockholm, 2004. 66.
[22] J.P. Richard, K. Melikov, E. Vives, C. Ramos, B. Verbeure, M.J. Gait, L.V. Chernomordik, B. Lebleu, Cell-penetrating peptides. A reevaluation of the mechanism of cellular uptake, J. Biol. Chem. 278 (2003) 585–590.
[23] W. Zhang, J. Song, B. Zhang, L. Liu, K. Wang, R. Wang, Design of acid-activated cell penetrating peptide for delivery of active molecules into cancer cells, Bioconjug. Chem. 22 (2011) 1410–1415.
[24] H. Myrberg, L. Zhang, M. Mae, U. Langel, Design of a tumor-homing cell-penetrating peptide, Bioconjug. Chem. 19 (2008) 70–75.
[25] A.W. Schuttelkopf, D.M. van Aalten, PRODRG: a tool for high-throughput crystallography of protein–ligand complexes, Acta Crystallogr. D 60 (2004) 1355–1363.
[26] D.M. York, T.A. Darden, L.G. Pedersen, The effect of long-range electrostatic interactions in simulations of macromolecular crystals—a comparison of the Ewald and truncated list methods, J. Chem. Phys. 99 (1993) 8345–8348.
[27] S.S. Wang, B.F. Gisin, D.P. Winter, R. Makofske, I.D. Kulesha, C. Tzougraki, J. Meienhofer, Facile synthesis of amino-acid and peptide esters under mild conditions via cesium salts, J. Org. Chem. 42 (1977) 1286–1290.
[28] G.R. Satpathy, Z. Torok, R. Bali, D.M. Dwyre, E. Little, N.J. Walker, F. Tablin, J.H. Crowe, N.M. Tsvetkova, Loading red blood cells with trehalose: a step towards biostabilization, Cryobiology 49 (2004) 123–136.
[29] M. Belting, Heparan sulfate proteoglycan as a plasma membrane carrier, Trends Biochem. Sci. 28 (2003) 145–151.
[30] E. Vives, C. Granier, P. Prevot, B. Lebleu, Structure–activity relationship study of the plasma membrane translocating potential of a short peptide from HIV-1 Tat protein, Lett. Pept. Sci. 4 (1997) 429–436.
[31] P.A. Wender, D.J. Mitchell, K. Pattabiraman, E.T. Pelkey, L. Steinman, J.B. Rothbard, The design, synthesis, and evaluation of molecules that enable or enhance cellular uptake: peptoid molecular transporters, Proc. Natl. Acad. Sci. U. S. A. 97 (2000) 13003–13008.
[32] D.J. Mitchell, D.T. Kim, L. Steinman, C.G. Fathman, J.B. Rothbard, Polyarginine enters cells more efficiently than other polycationic homopolymers, J. Pept. Res. 56 (2000) 318–325.
[33] F. Chiappori, I. Merelli, L. Milanesi, A. Marabotti, Static and dynamic interactions between GALK enzyme and known inhibitors: guidelines to design new drugs for galactosemic patients, Eur. J. Med. Chem. 63 (2013) 423–434.
[34] H. Brooks, B. Lebleu, E. Vives, Tat peptide-mediated cellular delivery: back to basics, Adv. Drug Deliv. Rev. 57 (2005) 559–577.
[35] W.C. Chan, P.D. White, Fmoc Solid Phase Peptide Synthesis: A Practical Approach, Oxford University Press, Oxford, 2000.
[36] F.F. Liu, X.Y. Dong, Y. Sun, Molecular mechanism for the effects of trehalose on beta-hairpin folding revealed by molecular dynamics simulation, J. Mol. Graph. Model. 27 (2008) 421–429.
[37] M.A. González, Force fields and molecular dynamics simulations, Collect. SFN 12 (2011) 169–200.
[38] W.L. Jorgensen, J. Tirado-Rives, Potential energy functions for atomic-level simulations of water and organic and biomolecular systems, Proc. Natl. Acad. Sci. U. S. A. 102 (2005) 6665–6670.
[39] F.F. Liu, L. Ji, X.Y. Dong, Y. Sun, Molecular insight into the inhibition effect of trehalose on the nucleation and elongation of amyloid beta-peptide oligomers, J. Phys. Chem. B 113 (2009) 11320–11329.
[40] M.A. Villarreal, S.B. Diaz, E.A. Disalvo, G.G. Montich, Molecular dynamics simulation study of the interaction of trehalose with lipid membranes, Langmuir 20 (2004) 7844–7851.
[41] L. Pol-Fachin, C.F. Becker, J.A. Guimaraes, H. Verli, Effects of glycosylation on heparin binding and antithrombin activation by heparin, Proteins 79 (2011) 2735–2745.
[42] L. Pol-Fachin, H. Verli, Depiction of the forces participating in the 2-O-sulfo-alpha-L-iduronic acid conformational preference in heparin sequences in aqueous solutions, Carbohydr. Res. 343 (2008) 1435–1445.
[43] E. Vives, P. Brodin, B. Lebleu, A truncated HIV-1 Tat protein basic domain rapidly translocates through the plasma membrane and accumulates in the cell nucleus, J. Biol. Chem. 272 (1997) 16010–16017.
[44] S. El-Andaloussi, P. Jarver, H.J. Johansson, U. Langel, Cargo-dependent cytotoxicity and delivery efficacy of cell-penetrating peptides: a comparative study, Biochem. J. 407 (2007) 285–292.
[45] D. Derossi, S. Calvet, A. Trembleau, A. Brunissen, G. Chassaing, A. Prochiantz, Cell internalization of the third helix of the antennapedia homeodomain is receptor-independent, J. Biol. Chem. 271 (1996) 18188–18193.
[46] F. Duchardt, M. Fotin-Mleczek, H. Schwarz, R. Fischer, R. Brock, A comprehensive model for the cellular uptake of cationic cell-penetrating peptides, Traffic 8 (2007) 848–866.
[47] M.M. Fretz, N.A. Penning, S. Al-Taei, S. Futaki, T. Takeuchi, I. Nakase, G. Storm, A.T. Jones, Temperature-, concentration- and cholesterol-dependent translocation of L- and D-octa-arginine across the plasma and nuclear membrane of CD34(+) leukaemia cells, Biochem. J. 403 (2007) 335–342.
[48] C.L. Watkins, D. Schmaljohann, S. Futaki, A.T. Jones, Low concentration thresholds of plasma membranes for rapid energy-independent translocation of a cell-penetrating peptide, Biochem. J. 420 (2009) 179–189.
[49] V.P. Torchilin, T.S. Levchenko, R. Rammohan, N. Volodina, B. Papahadjopoulos-Sternberg, G.G.M. D'Souza, Cell transfection in vitro and in vivo with nontoxic TAT peptide–liposome–DNA complexes, Proc. Natl. Acad. Sci. U. S. A. 100 (2003) 1972–1977.
[50] V. Torchilin, J. Babich, V. Weissig, Liposomes and micelles to target the blood pool for imaging purposes, J. Liposome Res. 10 (2000) 483–499.
[51] M. Akhoondi, H. Oldenhof, C. Stoll, H. Sieme, W.F. Wolkers, Membrane hydraulic permeability changes during cooling of mammalian cells, Biochim. Biophys. Acta 1808 (2011) 642–648.